

Exploring laser-induced interlayer spin transfer by an all-optical method

A. J. Schellekens, N. de Vries, J. Lucassen, and B. Koopmans*

*Department of Applied Physics, Center for NanoMaterials (cNM), Eindhoven University of Technology,
PO Box 513, 5600 MB Eindhoven, The Netherlands*

(Received 7 May 2014; revised manuscript received 16 July 2014; published 30 September 2014)

We investigate the influence of spin currents during ultrafast laser-induced demagnetization of magnetic bilayer structures by a new all-optical method to measure material- and/or depth-resolved magnetization dynamics. By describing the magneto-optical response of the bilayers in the complex Kerr plane, it is shown that the material-specific magnetization dynamics of the individual layers can be measured by a marginal adjustment to any conventional time-resolved magneto-optical Kerr effect setup. We use this technique to trace superdiffusive spin currents in magnetic Ni/Fe bilayers, providing new insight on its importance to ultrafast laser-induced demagnetization.

DOI: [10.1103/PhysRevB.90.104429](https://doi.org/10.1103/PhysRevB.90.104429)

PACS number(s): 75.78.Jp, 75.76.+j, 78.20.Ls

Since the discovery of ultrafast quenching of the magnetic order in ferromagnetic Ni by femtosecond (fs) laser pulses [1], the field of femtomagnetism has received widespread attention from the scientific community [2]. The observed strong nonequilibrium dynamics are not only of interest from a fundamental point of view, but also look promising for ultrafast all-optical control of magnetism in future applications. Recently, it was realized that apart from local mechanisms, also the laser-induced transfer of spin polarized carriers over several to tens of nanometers can be a source of ultrafast magnetization dynamics [3]. This notion triggered fascinating new studies [4–14], but also led to intense scientific debate. It was experimentally demonstrated that laser-induced demagnetization can be enhanced by transfer of spins aligned antiparallel to the magnetization direction [4]. Even more excitingly, it has been claimed that so-called superdiffusive spin currents can lead to an increase of the magnetization to a value larger than the saturation magnetization. Rudolf *et al.* reported on such an ultrafast magnetization enhancement in an Ni/Ru/Fe trilayer [6]. In this article, we demonstrate a new all-optical method to study ultrafast magnetic processes in a materials- and layer-specific way; shining new light on the experiment by Rudolf *et al.*

The most commonly used technique to study the ultrafast response of a ferromagnet is the time-resolved magneto-optical Kerr effect (TR-MOKE), where an intense pump pulse excites the ferromagnet and triggers the magnetization dynamics, which are subsequently studied by a probe pulse. As both the pump and probe pulse are generally shorter than 100 fs, this provides access to the magnetization dynamics on time scales shorter than the elementary processes governing them. However, in the case of multisublattice magnets or magnetic multilayers, the dynamics of the individual sublattices or layers cannot be disentangled, and the measured magneto-optical response is in general an average over all sublattices and/or layers. Therefore, it is no surprise that the study of ultrafast magnetization dynamics received a huge boost by the advent of fs x-ray pulses [15–17]. The main advantage of using x rays instead of MOKE is their element specificity; by tuning the x-ray energy to the absorption edge of an element,

only the dynamics of that specific element are measured. As an example, this provides the opportunity to study the nonequilibrium dynamics of ferro- and ferrimagnetic alloys [18,19]. In addition, it allowed for the quantification of spin transfer between two magnetic layers after pulsed laser excitation, such as was used in the earlier quoted study by Rudolf *et al.* [6,12].

There is, however, one major disadvantage of using x rays to study magnetization dynamics: they require large scale facilities for fs electron slicing or x-ray free electron lasers [7,9,16,18]. Recently, other techniques have been introduced to measure element-specific magnetization dynamics, such as table-top higher harmonic generation [20,21] or the performance of MOKE at different frequencies in the visible spectrum [22]. However, the equipment required for these techniques is expensive and depends on an accidental disappearance of the magneto-optical signal at a certain frequency of the laser light. Moreover, the higher harmonic generation approach does not allow for a full spectroscopic view on the circular magnetic dichroism because just a discrete set of spectral lines can be used, highlighting the need for other complementary methods. The technique introduced in this article provides such an alternative, and can be implemented in virtually any standard TR-MOKE setup. We use the Ni/Ru/Fe system to demonstrate our technique, and also to show that the role of superdiffusive spin currents is still far from understood.

Our technique to measure material-specific magnetization dynamics is based on the method proposed by Hamrle *et al.* [23], which is schematically depicted in Fig. 1. The magneto-optical (MO) response of a sample can be described as a vector Φ in the complex Kerr plane spanned by the ellipticity ε and rotation θ , with a specific Kerr angle ξ and Kerr amplitude R . This is schematically depicted in Fig. 1(a). In a structure with two magnetic films the total MO response of the sample Φ_{tot} is just the sum of the two Kerr vectors Φ_1 and Φ_2 . In a normal MO experiment either ε or θ is measured, which is simply the projection of the Kerr vector Φ on one of the two orthogonal axes. However, in principle one can also measure a linear combination of ε and θ , effectively rotating the projection axis P , as displayed in Fig. 1(b). By rotating the projection axis such that it is orthogonal to one of the individual Kerr vectors, this Kerr vector can be completely removed from the MO signal.

*b.koopmans@tue.nl

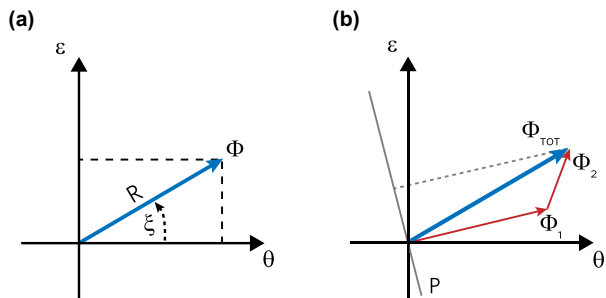


FIG. 1. (Color online) (a) Example of a Kerr vector Φ of a single magnetic layer in the plane spanned by the ellipticity ε and rotation θ . (b) Example of the total Kerr vector Φ_{tot} of a sample consisting of two individual layers with individual Kerr vectors Φ_1 and Φ_2 . On performing a measurement by projecting on the P axis, which is orthogonal to Φ_1 , only Φ_2 turns up in the magneto-optical signal.

To measure magnetization dynamics with material and/or depth sensitivity a setup is required where the projection axis P can be rotated, which can be accomplished in various ways [23,24]. Here, this is done by adding a quarter wave plate (QWP) to a standard double modulation TR-MOKE setup [25]. The setup is schematically depicted in Fig. 2. Here laser pulses coming from a Ti:sapphire laser (repetition rate 82 MHz, $\hbar\omega \approx 1.5$ eV) are split in a pump and a probe beam which are focused on the same position on the sample. At the sample the laser pulse length is ≈ 300 fs full width at half maximum (FWHM). The pump and probe beam are modulated by a mechanical chopper (≈ 60 Hz) and a photoelastic modulator (PEM) (≈ 50 kHz), respectively. Before the PEM, the probe beam is guided through a polarizer P at an angle of 45° with respect to the PEM easy axis, and through a QWP at an adjustable angle α . The reflected probe is passed through an analyzer A that is aligned to the main axis of the PEM, and its intensity is measured by a detector D . The signals at 50 kHz (V_{1f}) and 100 kHz (V_{2f}) are measured by a lock-in L1. Without the QWP it has been shown that $V_{1f} \sim \varepsilon$ and $V_{2f} \sim \theta$ [25], which means that by locking to the first (second) harmonic of the PEM, one is sensitive to $\varepsilon(\theta)$. However, in the aforementioned setup, the angle of the QWP determines whether the PEM modulates the light between two circularly polarized states (for $\alpha = 45^\circ$) or two linearly polarized states (for $\alpha = 0^\circ$), effectively switching the signals of V_{1f} and V_{2f} .

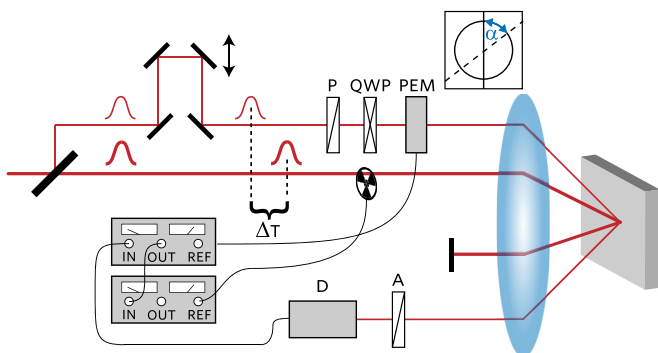


FIG. 2. (Color online) Double modulation TR-MOKE setup tailored for material and/or depth sensitivity by the addition of a quarter wave plate. See text for details.

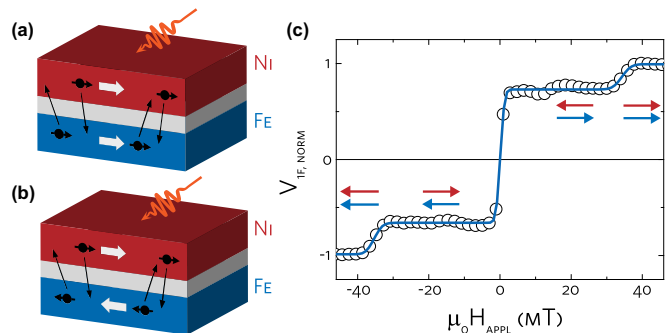


FIG. 3. (Color online) (a) and (b) show the basic concept of the experiments performed in this article. fs laser pulses induce spin currents between Ni and Fe. By measuring the magnetization dynamics of the Ni and Fe layer for parallel (a) and antiparallel (b) alignment, the contributions of these spin currents to the demagnetization process can be determined. (c) Typical branch of a hysteresis loop for the bilayer under investigation. The direction of the magnetization in the Ni and Fe layers are denoted by the arrows, displaying four different configurations of the bilayer structure.

This means that α determines whether one is sensitive to ε , θ , or a selected linear combination of both.

The measured MO response for the setup depicted in Fig. 2 can be calculated using the Jones formalism [26], resulting in the following relation:

$$\begin{pmatrix} V_{1f} \\ V_{2f} \end{pmatrix} \sim \begin{pmatrix} -(\sin 2\alpha)^2 & -\cos 2\alpha \\ -\cos 2\alpha & (\sin 2\alpha)^2 \end{pmatrix} \begin{pmatrix} \varepsilon \\ \theta \end{pmatrix}. \quad (1)$$

Although the matrix in Eq. (1) that relates ε and θ to V_{1f} and V_{2f} is not exactly a rotation matrix, it can be shown that for any arbitrary Kerr vector Θ there is an α such that the contribution of the specific Kerr vector to V_{1f} or V_{2f} is removed.

We will now continue to demonstrate that the setup shown in Fig. 2 can indeed be used for material-specific MOKE. To this extent we investigate the superdiffusive spin transport in structures similar to the ones investigated by Rudolf *et al.* [6], which are depicted in Figs. 3(a) and 3(b). Here, a Ni and Fe thin film are separated by a nonmagnetic spacer layer. By measuring the material-specific magnetization dynamics for the parallel (P) and antiparallel (AP) configuration the contributions of superdiffusive spin currents to the ultrafast demagnetization can be traced. In specific, we are interested in a possible *enhancement* of the magnetization of Fe due to spin transport after fs pulsed laser excitation, as surprisingly observed by Rudolf *et al.* [6].

The exact structure investigated is a Pt(4)/Fe(5)/Ru(1.2)/Ni(5)/Pt(1) magnetic bilayer. Here, the numbers denote the layer thickness in nanometers. The films are deposited by dc magnetron sputtering on a boron doped Si substrate, capped by a native oxide layer. The Pt bottom layer serves a buffer layer to induce proper growth of the magnetic bilayer structure, whereas the top Pt layer simply prevents oxidation of Ni after deposition. More importantly, the thickness of the Ru spacer layer is chosen such that Fe and Ni couple antiferromagnetically due to the Ruderman-Kittel-Kasuya-Yosida (RKKY) interaction [27].

Before measuring the magnetization dynamics, first static MOKE measurements are performed. This is done to check the magnetic properties of the samples, and to obtain the values of α at which only Ni or Fe contributes to the MO signal. A typical static MOKE measurement is shown in Fig. 3(c), where the applied field H_{appl} is swept from positive to negative values. The lines are fits of the data with three error functions. All measurements are performed with the magnetic field applied in the film plane and in the longitudinal MOKE setup. For small applied fields where the exchange energy exceeds the Zeeman energy of the Ni film, i.e., for $|H_{\text{appl}}| < 40$ mT, the bilayer will be in the AP configuration, and the magnetization of Fe will be parallel to H_{appl} . For larger fields, both Ni and Fe align to the field, and the P configuration is obtained. This means that four different configurations can be reached, as denoted by the arrows in Fig. 3(c).

We will now proceed to obtain the values of α where either Fe or Ni is effectively removed from the MO signal. To this extent, hysteresis loops like in Fig. 3(c) are measured for various α . Again, the data are fitted by error functions to obtain the contributions of Ni and Fe to the first harmonic V_{1f} , which we denote as $V_{1f,\text{Ni}}$ and $V_{1f,\text{Fe}}$, respectively. The results are depicted in Fig. 4(a), and fitted with Eq. (1). The fits yield reasonable agreement to the data, and the obtained Kerr angles are $\xi_{\text{Ni}} = 0.53\pi$ rad and $\xi_{\text{Fe}} = 0.22\pi$ rad, meaning that the Kerr rotation for Ni almost vanishes at the used wavelength. Because of the larger magnetic moment Fe will always be aligned to the magnetic field, and thus switches its orientation only once, as can be seen in Fig. 4(b). Ni changes its direction three times, because it aligns antiparallel to Fe when H_{appl} is smaller than the exchange field, but will align to the field when H_{appl} is largest.

To make sure that for the final time-resolved measurements the correct values of α are used, hysteresis loops are taken right before the measurements around the values of α indicated in Fig. 4(a). The loops show that $V_{1f,\text{Ni}}$ is virtually zero at $\alpha = -7^\circ$, and $V_{1f,\text{Fe}}$ is zero at $\alpha = 68^\circ$. To illustrate this, the hysteresis loops for these angles are plotted in Figs. 4(b) and 4(c), including the fits with the error functions. In Fig. 4(b), where the contribution from Ni should be absent in the MO signal, only one switch of the magnetization is visible, as expected when only Fe contributes to the MO signal. In Fig. 4(c) three steps are visible in the magnetization which are of equal size, corresponding to switching of the Ni layer.

Now that we have determined the values of α where only Ni or Fe contributes to the MO signal, the dynamics of the individual layers can be measured. For both Ni and Fe this is done for the four configurations of the magnetic bilayer. For the P configuration $H_{\text{appl}} = \pm 60$ mT is used, while for the AP configuration $H_{\text{appl}} = \pm 20$ mT. To remove any nonmagnetic contributions from the signal, the measurements at positive and negative fields are subtracted from each other, resulting in a purely magnetic time-resolved signal from either the Ni or Fe layer.

To present the genuine magnetization dynamics of the Ni and Fe films, first state filling effects are removed by fitting the raw data with an analytical solution of the three temperature model (3TM) in the low fluence limit [28]. The resulting demagnetization curves are plotted in Figs. 5(a) and 5(b) for Ni and Fe, respectively, where the lines denote

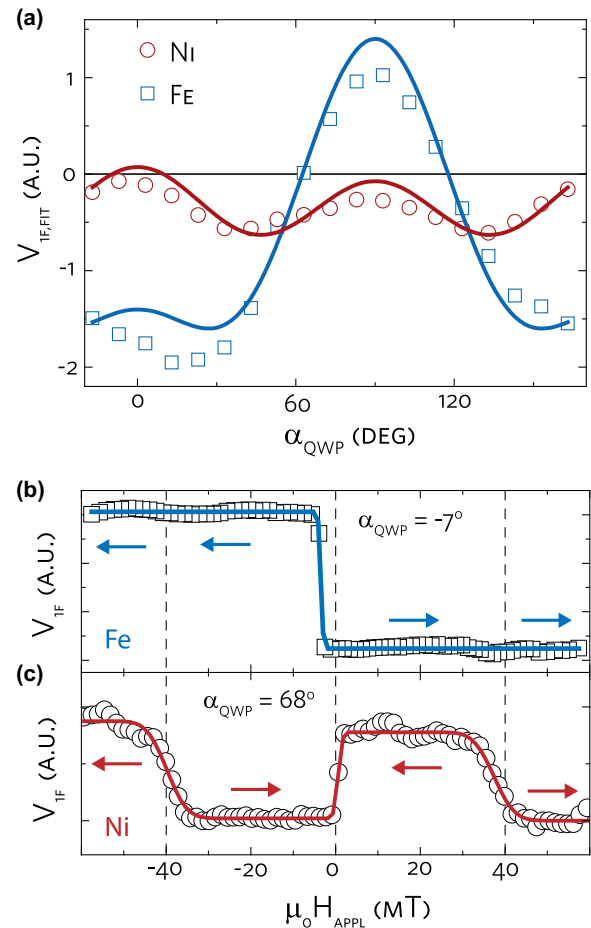


FIG. 4. (Color online) (a) Measured values of V_{1f} for Fe and Ni as obtained from fitting hysteresis loops as a function of α . The lines are fits to Eq. (1). In (b) one branch of a hysteresis loop is shown for $\alpha = -7^\circ$, showing only a contribution from Fe to the MO contrast. In (c) the same is shown at $\alpha = -68^\circ$, where only a contribution from Ni is seen.

fits with the same analytical solution of the 3TM. Let us first discuss the data for Ni in Fig. 5(a), where a very clear difference between the P and AP configuration is observed. In the case of P alignment, the maximum demagnetization is 45% larger than in the AP case. Furthermore, the delay time at which the maximum demagnetization is reached, indicated by the vertical bars, is 350 fs for AP alignment compared to 580 fs for P alignment. In other words, the demagnetization in the P alignment is slower and less effective. This corresponds to the observations by Rudolf *et al.* [6], and could be caused by superdiffusive spin transport from the Fe to the Ni layer, slowing down or speeding up the demagnetization process. From the measurements it can be estimated that roughly 30% of the observed demagnetization of Ni is caused by superdiffusive spin currents from the Fe layer. A large difference between the measurements presented in the literature [6], is that after 1.5 ps the demagnetization is approximately equal for the P and AP configuration, showing that the system returns to thermal equilibrium rapidly after the nonequilibrium spin currents have vanished, similar to previous observations in the literature [4,29].

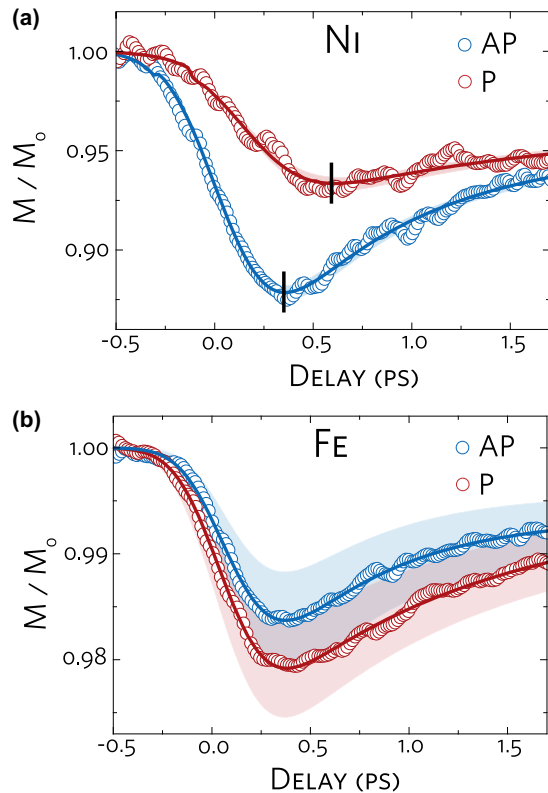


FIG. 5. (Color online) Demagnetization traces of Ni (a) and Fe (b) for the P and AP configuration of the magnetic bilayer. The lines are fits with an analytical solution of the three temperature model [28], while the upper bounds for the errors due to mixing of the Ni and Fe signals are indicated by the shaded areas. For Ni the time for maximum demagnetization is indicated by vertical bars. While for Ni a significant change in the demagnetization properties is observed between the P and AP configuration, the traces for Fe are almost identical.

We now turn our attention to the response of the Fe layer in Fig. 5(b). Unlike earlier reports, a clear demagnetization is observed for the P configuration, instead of the surprising enhancement. More strongly, qualitatively the observed demagnetization traces are virtually identical, and only a slightly larger demagnetization is observed in the P alignment. This change in the demagnetization of the Fe layer cannot be attributed to spin currents from the Ni layer, as this would yield a larger demagnetization in the AP case. Instead, we believe that the small differences between the traces are caused by a measurement artifact rather than by a physical phenomenon. Because the demagnetization of the Ni layer is much larger than that of the Fe layer (≈ 5 times), a very small contribution from Ni to the MO signal could fully explain the differences

between the AP and P configuration. Therefore, the upper boundaries of the errors due to mixing of the signals are estimated from the hysteresis loops, and depicted by shaded areas in Figs. 5(a) and 5(b). While for Ni the errors are so small that the areas are hardly visible, for Fe they overlap for the AP and P case. This means that the observed differences could indeed be caused by a small ($V_{\text{if,Ni}} \approx \frac{1}{40} V_{\text{if,Fe}}$) contribution of Ni to the Fe signal. Finally, one might argue that the contributions of Ni to the measurements of Fe hide a possible enhancement of the magnetization. However, the maximum contributions of Ni to Fe, as indicated by the shaded areas in Fig. 5(b), should be four times larger than estimated, which is extremely unlikely.

The measurements presented in this article using all-optical depth-resolved MOKE do not confirm that a long-lived ferromagnetic state is present after fs pulsed laser excitation of a magnetic bilayer, contrary to observations with other techniques. We will now speculate on possible reasons for these differences. First of all, the samples used in the present measurements were not identical to the ones investigated by higher harmonic generation by Rudolf *et al.* [6]. Most importantly, instead of a Ta buffer layer a Pt buffer layer was used, however, this is not expected to significantly change the observed dynamics, as the spin diffusion lengths in both materials are approximately equal [30]. Another difference which might be important, is the laser fluence. Here, the magnetization of Ni is only quenched by $\sim 10\%$, while Rudolf *et al.* used fluences to quench the magnetization up to 60%. Although it was claimed that superdiffusive spin transport is especially effective in the low-fluence regime [3], recent experiments on CoFeB/MgO/CoFeBo show that the relative contributions of transport increase for larger laser fluences [29]. We therefore plan to perform a systematic study as a function of fluence using an amplified laser system in the near future.

Concluding, we introduced a flexible technique to measure material-specific magnetization dynamics with MOKE. The technique is applied to study the heavily debated role of spin transport in magnetic bilayer structures. Although transport effects are shown to play a large role in the investigated samples (up to 30% for Ni), the enhancement of the magnetization of Fe in the literature could not be reproduced for the used laser fluences. This shows that the role of transport during ultrafast demagnetization is still far from understood. We believe that material-specific MOKE will prove to be an important tool for future studies on spin transport during ultrafast demagnetization, and might even be employed for the study of element-specific magnetization dynamics in multisublattice magnets.

This work was supported by the Foundation for Fundamental Research on Matter (FOM), which is part of the Netherlands Organization for Scientific Research (NWO).

-
- [1] E. Beaurepaire, J.-C. Merle, A. Daunois, and J.-Y. Bigot, *Phys. Rev. Lett.* **76**, 4250 (1996).
 [2] A. Kirilyuk, A. V. Kimel, and T. Rasing, *Rev. Mod. Phys.* **82**, 2731 (2010).
 [3] M. Battiato, K. Carva, and P. M. Oppeneer, *Phys. Rev. Lett.* **105**, 027203 (2010).
 [4] G. Malinowski, F. Dalla Longa, J. H. H. Rietjens, P. V. Paluskar, R. Huijink, H. J. M. Swagten, and B. Koopmans, *Nature Phys.* **4**, 855 (2008).
 [5] A. Melnikov, I. Razdolski, T. O. Wehling, E. Th. Papaioannou, V. Roddatis, P. Fumagalli, O. Aktsipetrov, A. I. Lichtenstein, and U. Bovensiepen, *Phys. Rev. Lett.* **107**, 076601 (2011).

- [6] D. Rudolf *et al.*, *Nature Comm.* **3**, 1037 (2012).
- [7] T. Wang *et al.*, *Phys. Rev. Lett.* **108**, 267403 (2012).
- [8] B. Vodungbo *et al.*, *Nature Comm.* **3**, 999 (2012).
- [9] B. Pfau *et al.*, *Nature Comm.* **3**, 1100 (2012).
- [10] A. J. Schellekens, W. Verhoeven, T. N. Vader, and B. Koopmans, *Appl. Phys. Lett.* **102**, 252408 (2013).
- [11] A. Eschenlohr *et al.*, *Nature Mat.* **12**, 332 (2013).
- [12] E. Turgut *et al.*, *Phys. Rev. Lett.* **110**, 197201 (2013).
- [13] B. Pfau *et al.*, *Nature Comms.* **3**, 1100 (2012).
- [14] N. Moisan *et al.*, *Sci. Rep.* **4**, 4658 (2014).
- [15] R. W. Schoenlein, S. Chattopadhyay, H. H. W. Chong, T. E. Glover, P. A. Heimann, C. V. Shank, A. A. Zholents, and M. S. Zolotarev, *Science* **287**, 2237 (2000).
- [16] C. Stamm *et al.*, *Nat. Mater.* **6**, 740 (2007).
- [17] H. A. Dürr, T. Eimüller, H.-J. Elmers, S. Eisebitt, M. Farle, W. Kuch, F. Matthes, M. Martins, H.-C. Mertins, P. M. Oppeneer, L. Plucinski, C. M. Schneider, H. Wende, W. Wurth, and H. Zabel, *IEEE Trans. on Magn.* **45**, 15 (2009).
- [18] I. Radu *et al.*, *Nature (London)* **472**, 205 (2011).
- [19] S. Mathias *et al.*, *Proc. Natl. Acad. Sci. USA* **109**, 4792 (2011).
- [20] C. La-O-Vorakiat, E. Turgut, C. A. Teale, H. C. Kapteyn, M. M. Murnane, S. Mathias, M. Aeschlimann, C. M. Schneider, J. M. Shaw, H. T. Nembach, and T. J. Silva, *Phys. Rev. X* **2**, 011005 (2012).
- [21] S. Mathias, C. La-o-vorakiat, J. M. Shaw, E. Turgut, P. Grychtol, R. Adam, D. Rudolf, H. T. Nembach, T. J. Silva, M. Aeschlimann, C. M. Schneider, H. C. Kapteyn, and M. M. Murnane, *J. Electron Spectrosc. Relat. Phenom.* **189**, 164 (2013).
- [22] A. R. Khorsand, M. Savoini, A. Kirilyuk, A. V. Kimel, A. Tsukamoto, A. Itoh, and Th. Rasing, *Phys. Rev. Lett.* **110**, 107205 (2013).
- [23] J. Hamrle, J. Ferré, M. Nývlt, and Š. Višňovský, *Phys. Rev. B* **66**, 224423 (2002).
- [24] J. Ferré, P. Meyer, M. Nývlt, S. Visnovsky, and D. Renard, *J. Magn. Magn. Mater.* **165**, 92 (1997).
- [25] B. Koopmans, M. van Kampen, J. T. Kohlhepp, and W. J. M. de Jonge, *J. Appl. Phys.* **87**, 5070 (2000).
- [26] R. C. Jones, *J. Opt. Soc. Am.* **31**, 488 (1941).
- [27] K. Yosida, *Phys. Rev.* **106**, 893 (1957).
- [28] F. Dalla Longa, J. T. Kohlhepp, W. J. M. de Jonge, and B. Koopmans, *Phys. Rev. B.* **75**, 224431 (2007).
- [29] W. He, T. Zhu, X.-Q. Zhang, H.-T. Yang, and Z.-H. Cheng, *Sci. Rep.* **3**, 2883 (2013).
- [30] C. Hahn, G. de Loubens, O. Klein, M. Viret, V. V. Naletov, and J. Ben Youssef, *Phys. Rev. B* **87**, 174417 (2013).